


Evaluation of a bioprinted 3D airway tissue model for toxicity testing of nanomaterials; Pathway to integration into a tiered testing strategy for hazard assessment to support safety-by-design

Yunji Lee ^a, Katie McAllister ^b, Hwa-Rim Lee ^a, Sungjune Jung ^{a,*}, Fiona Murphy ^{b,*} 

^a Department of Materials Science and Engineering, Pohang University of Science and Technology (POSTECH), Pohang, Republic of Korea

^b Strathclyde Institute of Pharmacy and Biomedical Sciences, University of Strathclyde, Glasgow, Scotland, United Kingdom

ARTICLE INFO

Keywords:

Bioprinted 3D tissue models
Nanomaterial hazard assessment
in vitro alternatives
Safer-by-Design

ABSTRACT

There is an urgent need to identify hazards posed by novel nanomaterials (NMs), however, new models are required to streamline testing approaches, increase our understanding of mechanism of toxicity and incorporate Safer-by-Design concepts into NM development. Here, we conducted an evaluation of a sophisticated 3D bioprinted airway model for a first-in-kind hazard assessment of NMs. Exploiting the consistency and reproducibility provided by bioprinting techniques, airway constructs were generated by precisely controlled sequential layering of endothelial cells, fibroblasts embedded in collagen, and bronchial epithelial cells and exposed to ZnO and BaSO₄ NMs case-study materials. Exposure to ZnO resulted in greater temporal and dynamic immunotoxic and histological responses in contrast to BaSO₄, demonstrating the successful differentiation of high and low reactivity NMs. Comparison with simple *in vitro* toxicity studies and existing *in vivo* and human data demonstrated the physiological relevance of increasing model complexity. The relative benefits of the 3D bioprinted airway model and potential for inclusion in tiered testing strategies was substantiated by comprehensive review of the current state-of-the-art alternative models. This study supports the wider adoption of a sophisticated *in vitro* airway model to reduce our reliance on *in vivo* testing and advance efforts to develop Integrated Approaches to Assessment and Testing to support Safer-by-Design NM innovation.

Background

Over the last decade there has been a notable rise in nanomaterial (NM) development and production for a vast array of different applications increasing concerns of the impact on human health. The vast number of different NMs in production and under development precludes the complete hazard assessment of each individual substance according to current regulatory standards which are based on long term *in vivo* studies [1]. This has stimulated efforts to design alternative strategies to streamline the risk assessment process [2] based on integration of hazard data from a variety of sources into tiered testing strategies which promote preferential use of *in silico* modelling, *in chemico* and acellular assays and *in vitro* models before progressing to *in vivo* studies. (Fig. 1).

However for these strategies to gain wider acceptance and eventually serve to reduce the burden of animal testing in toxicology the unmet need for morphologically and functionally relevant, yet reliably

manufacturable and reproducible *in vitro* models of human airways to precede *in vivo* testing must first be met [3-5]. Currently, simple 2D cell monocultures are the predominant models used in the safety assessment of inhaled particles to address human health concerns, however, these systems fail to replicate the complexity of the lung tissue. Identifying particles with the potential to cause complex and chronic diseases after exposure via inhalation, such as fibrosis and lung cancer, requires an understanding of how interactions between particles and target cells stimulate pro-inflammatory and pro-fibrotic changes leading to pathology, but also how multiple cell types present locally in the target tissue and within systemic systems contribute to the disease microenvironment, as crucial drivers of disease. The critical interactions between different cell types and tissue structure in response to toxic agents cannot be replicated in simple 2D cell monoculture models [6]. As a result, animal models are relied upon to confirm whether inhaled particles pose a hazard to human health.

Although recently significant progress has been made in the

* Corresponding authors.

E-mail addresses: sjjung@postech.ac.kr (S. Jung), f.murphy@strath.ac.uk (F. Murphy).

<https://doi.org/10.1016/j.nantod.2025.102655>

Received 20 May 2024; Received in revised form 21 November 2024; Accepted 26 January 2025

Available online 3 February 2025

1748-0132/© 2025 The Author(s). Published by Elsevier Ltd. This is an open access article under the CC BY license (<http://creativecommons.org/licenses/by/4.0/>).

development of multicell 3D models which mimic the cellular constituents of tissues and organs, it is not feasible to replicate the full complexity of the lung tissue. Each model therefore has specific limitations in terms of physiological relevance e.g., few models under development concomitantly consider the functional role of the extracellular matrix (ECM) in determining the tissue microenvironment and behaviour of cells [7,8]. Recognition that the lack of ECM biological motifs and discrepancies between the mechanical features of current airway models, such as the higher stiffness of the tissue culture dishes compared to the lung parenchyma, i.e. 10^6 kPa vs. 1–15 kPa, significantly influences cellular phenotype [9], has provided the impetus to develop and employ more physiologically relevant models for NM hazard that go beyond the current state-of-the-art [10].

Safe(r)-by-Design (SbD) NM development aims to reduce the human and environmental risk of a substance throughout its entire life cycle by minimizing or eliminating the hazard and/or by reducing exposure [11]. SbD testing can identify hazard warnings in the early stages of the innovation process using simple *in vitro* methods which balance predictivity, speed and cost for early-stage screening of multiple NMs to select candidates for further development and investment [12].

In this paper we evaluated the predictivity of a novel 3D bioprinted multicell model of the airway tissue for use in the hazard screening of NMs. Composed of lung endothelium, fibroblasts embedded in collagen ECM, and human airway derived epithelial cells the multicell 3D bioprinted airway model presented here effectively recapitulates a lower respiratory system with a high degree of physiological relevance [13]. By exploiting the consistency provided by bioprinting techniques to generate highly reproducible airway tissues, this approach advances the currently available models for hazard assessment and, when coupled with the relative simplicity in design, maintains the potential for application in high/medium throughput process as required to support SbD innovation [14].

Our previous studies using lung models constructed in a similar manner, have already indicated the potential use of this model for understanding lung tissue responses to viral infection [13,15,16], assessing toxicity of dust particles [17], and evaluating drug efficacy [18]. This model has been shown to replicate early markers of pulmonary fibrosis in response to toxic insult, however the responses after exposure to NMs have not yet been assessed. Therefore, in this pilot study we exposed the 3D bioprinted airway model to two NMs, ZnO (NM-110) and BaSO₄ (NM-220). Responses were then compared to results from simple *in vitro* epithelial monocultures and existing *in vivo* data to assess predictivity of hazard potential. ZnO NM-110 and BaSO₄ NM-220 were selected as well-characterised high and low reactivity NMs, respectively based on the wealth of toxicity available data from the literature. Both specific NMs have been previously included in a number of EU-funded consortia

projects (including MARINA, NanoReg, NanoReg2, GRACIOUS, PATROLS). ZnO NM-110 is also an OECD Working Party on Manufactured Nanomaterials (WPMN) case study NM. Together these efforts have generated a significant evidence base detailing the physicochemical characteristics, *in vitro* and *in vivo* toxicity of these NMs which is widely described in the literature and publicly accessible through NM databases such as eNanoMapper [19]. *In vitro* and *in vivo* studies have consistently reported acute cytotoxicity and inflammatory response to ZnO NM-110 exposure, whereas BaSO₄ NM-220 is generally considered to be relatively inert [20–22]. Therefore, we consider ZnO NM-110 and BaSO₄ NM-220 pertinent case study materials with which to test the applicability of this model for hazard assessment of NMs.

Selection of endpoints related to cell viability, cytotoxicity, oxidative stress and pro-inflammatory changes comply with the scientific advice [23] on fulfilling information requirements for nanomaterials under the EU REACH regulation (Registration, Evaluation, Authorisation of Chemicals, 2006) and are considered key to assess human hazard concerns [14].

A second objective of this project was to critically review the strengths and limitations of the model presented here in comparison with the leading alternative complex *in vitro* airway models used for NM hazard studies as reported in the literature. Based on the above, we hypothesized the 3D bioprinted airway model would be a useful addition to an integrated and tiered testing strategy for hazard assessment of NMs addressing the existing gap in physiologically relevant *in vitro* models which precede *in vivo* testing [24]. The inclusion in a tiered testing strategy will amplify the impact of the model described and greatly enhance the development and maturation of next-generation testing strategies for NM hazard assessment which are less reliant on *in vivo* testing.

Methods

Cell culture and bioink formulation

The HULEC-5a cell line (ATCC, VA, USA), representing human lung microvascular endothelial cells, was cultured in MCDB 131 medium (Thermo Fisher Scientific, MA, USA) supplemented with 10 % (v/v) fetal bovine serum (FBS; Cytiva, MA, USA), 1 % (v/v) antibiotic/antimycotic solution (Cytiva), 10 ng/mL human EGF recombinant protein (Thermo Fisher Scientific), 10 mM L-glutamine (Sigma-Aldrich, MO, USA), and 1 µg/mL hydrocortisone (Sigma-Aldrich). A cell density of 6×10^5 cells/mL HULEC-5a was suspended in complete MCDB 131 medium to generate the cell-laden ink for the initial layer of airway model. The MRC-5 cell line (ATCC), representing human lung fibroblasts, was propagated using MEM alpha modification (Cytiva) supplemented with

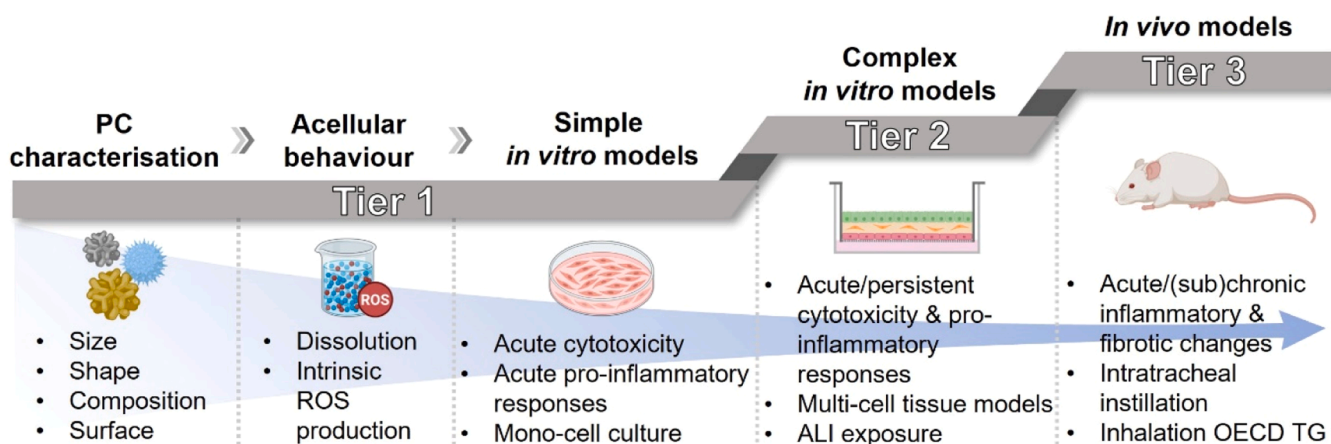


Fig. 1. Tiered testing strategy to support the Inhalation IATA adapted from Braakhuis et al. [14]. (PC: physicochemical; ROS: reactive oxygen species; ALI: air-liquid interface; TG: test guideline).

10 % FBS and 1 % antibiotic/antimycotic solution. MRC-5 cells at a concentration of 9×10^5 cells/mL were suspended in a 0.3 % (w/v) collagen solution to prepare the cell-laden ink for the second layer of the airway model. The collagen solution was composed of 0.375 % (w/v) atelocollagen (Dalimtissen, Republic of Korea), dissolved in 0.1 % (v/v) acetic acid solution. Following dissolution, the 0.375 % atelocollagen solution, 10X reconstitution buffer, and 10X nutrient buffer were mixed at an 8:1:1 vol ratio to create a 0.3 % (w/v) collagen solution with a neutral pH and sufficient nutrient for cells. Calu-3 cell line (ATCC), representing human lung epithelial cells, was expanded in RPMI 1640 medium (Cytiva) supplemented with 10 % FBS and 1 % antibiotic/antimycotic solution. A cell density of 4×10^5 cells/mL Calu-3 was suspended in complete RPMI 1640 medium to generate the cell-laden ink for the third layer of the airway model. For 2D cell experiments, Calu-3 cells were seeded in 96-well cell culture plates (Corning, UK) at a density of 1×10^5 cells/well in complete RPMI 1640 medium and incubated overnight before exposure with dose range of NMs.

Printing three-layered airway model

A pneumatic microextrusion printing system (ML-5000XII, Musashi, Japan) combined with 24 G nozzle (Musashi, Japan) was utilized to construct three-layered airway model. The first layer involved printed 0.5 mL HULEC-5a cell ink containing 3×10^5 cells onto a 12 mm cell culture insert, Transwell® (Corning, NY, USA) featuring a 0.4 μ m pore polycarbonate membrane. Immediately after printing the first layer, 1 mL of MCDB 131 medium was added beneath the insert, and the printed endothelial cells were left to incubate overnight. After removing the apical medium, 0.2 mL of MRC-5-laden collagen solution containing 1.8×10^5 MRC-5 cells was printed onto the endothelial layer. The collagen was then crosslinked through a 4 h incubation at 37°C. The third layer was created by printing 2×10^5 Calu-3 cells (0.5 mL) on the collagen layer. The culture medium for the airway model was a 1:1:1 mixture (volume ratio) of MCDB 131: MEM alpha: RPMI 1640, supplemented with 17 μ g/mL aprotinin (Roche, Germany) to prevent collagen contraction. To ensure stable cell binding to each layer, the models were initially cultured under submerged conditions for the first 4 days followed by air-liquid interface (ALI) culture until use. Daily medium changes were implemented throughout the culture period. Typically, we employ the airway model following a total culture period of 7–10 days.

Rheological analysis

The rheological properties of the bioinks were evaluated using a rheometer (Discovery HR 20, TA Instruments, DE, USA) equipped with a 60 mm diameter parallel plate. Viscosity was measured through a shear rate sweep ranging from 10 to 10,000 1/s. The storage modulus (G') and loss modulus (G'') were determined by conducting a frequency sweep from 10 to 100 rad/s at a constant strain of 1 %. All measurements were performed at 25°C.

Mechanical property

A 0.5 mL of 0.3 % (w/v) collagen solution was injected into a 12 mm Transwell and thermally crosslinked for 4 h at 37°C. The resulting disc-shaped hydrogels were then positioned between the bottom plates (at 37°C) and the 20 mm parallel plate of the rheometer (Discovery HR 20). Axial compressions were applied at a constant rate of 20 μ m/s until failure occurred. The compressive modulus was determined from the linear region of the strain-stress curve, within a strain range of 0–20 %.

Nanomaterial preparation

ZnO (NM-110) was provided by the NM repository at the Joint Research Center (JRC) and BaSO₄ (NM-220) was provided by the NM repository at the Fraunhofer Institute (IME). The physicochemical

intrinsic and extrinsic characteristics of each NM are detailed in [Tables S1](#), 2. ZnO NMs and BaSO₄ NMs were individually dispersed in phosphate buffered saline (PBS; Cytiva) containing 0.05 wt% bovine serum albumin (BSA; Sigma-Aldrich) to prevent NM aggregation 1 h prior to treatment. A 100 μ L NM solution was introduced into the apical side of the airway model, where medium was already present in the basolateral compartment. Within 1 day, the entire apical solution was released into the basolateral part, establishing a presence of NMs in the apical region conducive to ALI culture. The negative control group was treated with 100 μ L of PBS with 0.05 wt% BSA. The basal medium was collected for ELISA every 2 days and replaced with fresh medium. In 2D model NMs were prepared as above, media was removed from cell surface and replaced with 100 μ L NM suspension for 24 and 72 h.

Cell viability assay

To evaluate the cellular metabolic activity of the airway models, a Cell Counting Kit-8 (CCK-8) assay was conducted on day 3 post-NP treatment. The CCK-8 reagent was mixed with the medium at a 1:10 ratio to create a working solution. Following three times wash with PBS, 0.4 mL of the working solution was added to both the apical and basolateral sides of the model. Blank samples, consisting of NP-treated bare Transwell without tissue, were included to assess NP effects on colorimetric analysis. After 7 min incubation at 37°C, the solution was transferred to a 96-well plate (100 μ L, triplicate), and the absorbance of the medium was measured at 450 nm using a plate reader (Spark, Tecan Life Sciences, Switzerland). Cell viability was assessed in 2D culture by Neutral red uptake assay (TOX-4, Sigma-Aldrich) according to the manufacturer's instruction. Metabolic activity was assessed using alamarBlue™ Cell Viability Reagent (Thermo Fisher Scientific) and intracellular reactive oxygen species (ROS) production was measured after 30 min incubation with 1 μ M DCFH₂-DA probe (Sigma-Aldrich).

Histology

The airway model was fixed using 4 % paraformaldehyde dissolved in 1X PBS for 15 min at room temperature. Subsequently, the tissue on the porous membrane was cut out from the Transwell and embedded in optimal cutting temperature (OCT) compound (Leica Biosystems, Germany) before being frozen at –80°C. Frozen sections, 10 – 15 μ m thickness, were obtained using a microtome-cryostat (CMI860, Leica Biosystems). For histological examination, these sections were stained with hematoxylin (Mayer's, Dako, CA, USA) and eosin Y (Merck, Germany). To perform Alcian blue staining, the sectioned samples underwent staining with Alcian blue (Sigma-Aldrich), along with Nuclear fast red (Sigma-Aldrich). Apoptotic cells were identified using the TdT-mediated dUTP nick-end labelling (TUNEL) assay following the guidelines provided by the DeadEnd™ Fluorometric TUNEL System (Promega, WI, USA). The nuclei were concurrently stained with 0.2 μ g/mL Hoechst 33342 (Thermo Fisher Scientific) for 10 min. For immunofluorescence analysis of the sectioned samples, they were subjected to blocking using 5 % FBS and 0.2 % Triton X-100 (Sigma-Aldrich) in PBS. The samples were then exposed to the primary antibody targeting integrin β 1 (1:1000, ab24693, Abcam, UK) at room temperature for 4 h. Subsequently, the samples underwent incubation with the goat anti-mouse, Alexa 594-conjugated secondary antibody (1:200, A11032, Thermo Fisher Scientific) at room temperature for 1 h. Nuclei were counter-stained with 0.2 μ g/mL Hoechst 33342 for 10 min at room temperature.

Trans-epithelial electrical resistance (TEER) measurement

A volt-ohm meter (EVOM2, World Precision Instruments, FL, USA) equipped with double chopstick electrodes (STX2-Plus, World Precision Instruments) was utilized to measure TEER at room temperature. Before measurement, the medium was replaced with pre-warmed Dulbecco's

phosphate buffered saline (DPBS; Cytiva), with 0.5 mL on the apical side and 1 mL in the basolateral chamber. The TEER of the 3D printed airway model ($TEER_{Tissue}$) was determined using the equation provided below. $TEER_{Net}$ represents the TEER of the Transwell covered with the airway model, and $TEER_{Transwell}$ is the TEER of blank Transwell without cells.

$$TEER_{Tissue} [\Omega \cdot cm^2] = (TEER_{Net} - TEER_{Transwell}) [\Omega] \times \text{surface area } [cm^2]$$

Gene expression analysis

The airway models were rinsed with PBS and collected in e-tubes. After centrifugation, the resulting pellets underwent treatment with RNeasy Mini Kit (Qiagen, Germany) to extract total RNA, and the RNA concentrations were assessed using UV-Vis spectrophotometer (NanoDrop One, Thermo Fisher Scientific). The complementary DNA (cDNA) was synthesized using an oligo-dT primer and the High-Capacity cDNA Reverse Transcription Kit (Applied Biosystems, CA, USA). Gene expression levels were evaluated using a real-time PCR system (StepOne Plus, Thermo Fisher Scientific) with SYBR Green Master Mix (Thermo Fisher Scientific) and gene-specific primers (Table S3). The expression levels of the target genes were normalised to glyceraldehyde 3-phosphate dehydrogenase (GAPDH).

Statistical analysis

Quantitative data was presented using means and error bars representing standard deviation. The statistical significance of the values was assessed through a two-tailed *t*-test using the VassarStats website (www.vassarstats.net). The figure legends provide information on the sample sizes for each data set.

Results and discussion

Construction of the 3D bioprinted airway tissue model

The primary objective of this study was to evaluate a 3D bioprinted airway tissue model for use in NM hazard assessment (Fig. 2a). The airway tissue model was constructed by the sequential deposition of endothelial cells (HULEC-5a), fibroblast-containing collagen (MRC-5 cells), and bronchial epithelial cells (Calu-3) by bioprinting onto a permeable Transwell membrane (Fig. 2b). The rheological properties of each bioink, including viscosity and storage and loss moduli, were characterised using a rheometer (Figure S1). All the bioinks demonstrated suitable printability with a microextrusion bioprinter. The crosslinked collagen hydrogel used in this system exhibited a compressive modulus of 1.39 kPa, which falls within the range of the *in vivo* mechanical properties of lung tissue (Figure S2). After 7 days of ALI culture, the final bioprinted models had a three-layered structure with a thickness of approximately 30 μm and consisted of an endothelium, a basement membrane, and an epithelium replicating the basic tissue structure of the airway epithelium (Fig. 2c).

The epithelium of the tissues was exposed to various concentrations of ZnO (NM-110) or BaSO₄ (NM-220) NMs dispersed by ultrasonication in 0.5 % BSA/PBS (Fig. 2d, e). An initial dose-range finding study showed no measurable acute cytotoxicity after 24 h exposure up to concentrations of 156.25 $\mu\text{g}/\text{cm}^2$ of either ZnO or BaSO₄ (Figure S3); subsequent experimental exposure concentrations were set at 2.5, 10 and 25 $\mu\text{g}/\text{cm}^2$ in line with previously reported *in vitro* studies [25] and to replicate more realistic *in vivo* exposures. Airway tissue model responses to NM exposure were measured up to 14 days-post exposure.

The establishment of reliable and robust *in vitro* models for hazard assessment, a prerequisite for moving away from animal testing, requires a high degree of model reproducibility. The layered structure of

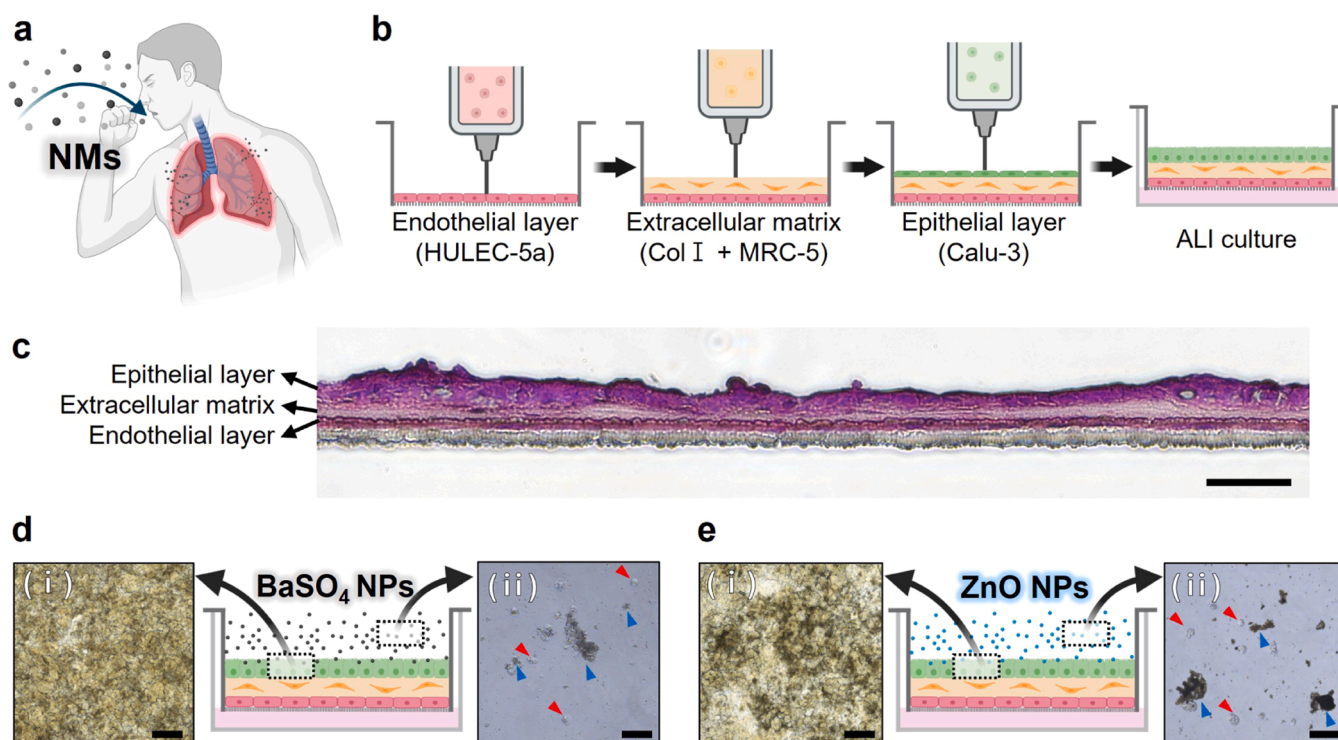


Fig. 2. Bioprinting of a 3D airway model and exposure to nanomaterials (NMs). a) Schematic illustration depicting the inhalation of NMs through the respiratory tract. b) The construction of a three-layered airway model using microextrusion bioprinting. Following fabrication, the model was cultured under air-liquid interface (ALI) conditions. c) Histological analysis of printed airway tissue after 7 days of ALI culture, visualized through hematoxylin and eosin (H&E) staining (scale bar = 50 μm). d, e) Exposure of the epithelial layer to BaSO₄ and ZnO nanomaterials (NMs). (i) Top view of the NM-deposited epithelial layer, and (ii) apical washing with PBS after 7 days of NM treatment. (Red arrow indicates dead cells; blue arrow indicates NMs) (scale bar = 100 μm).

this model was constructed by highly controlled bioprinting which allowed for consistent and reproducible replicates to be generated over a short period of time; ensuring the consistency in model generation, crucial for reliability of results obtained.

Histological changes induced by NM exposure

Tissue structures were visualized by H&E staining after 3-, 7-, and 14-days of exposure (Fig. 3). A noticeable increase in thickness of tissue was observed over time in all conditions with florid protrusions of the Calu-3 epithelial cell layer particularly evident in all NM-treated tissues. Interestingly, severe detachment of the Calu-3 layer occurred in response to NM exposure however delamination of the epithelial layer did not correspond with widespread loss of epithelial integrin (Figure S4). Alcian blue staining showed no changes in mucin production across treatment groups at any time point (Figure S5).

A dose-dependent increase in gene expression levels of proliferation marker, Ki67 was observed after 3-days of exposure to ZnO NM compared to control (Fig. 4a), highlighting the early stimulatory effect

of ZnO NM exposure on cell growth. Barrier formation was assessed by measurement of gene expression levels of the tight junction marker protein ZO-1, which was significantly increased after exposure to ZnO NM at day 3 but decreased after exposure to BaSO₄ (Fig. 4b). TEER was then used to assess functional barrier integrity over time. Control TEER values increased over time consistent with the observed increase in tissue thickness. Higher TEER values were recorded in tissue exposed to BaSO₄ at each time point compared to control. All exposure concentrations of ZnO NM caused an increase in TEER from 3 to 7 days of exposure, however high-dose ZnO NM exposure resulted in an apparent decrease in TEER at day 14 (Fig. 4c).

TUNEL staining was used to measure apoptotic cell death after NM exposure. No apoptotic cells were observed in control or BaSO₄ exposed tissues analysed at any dose or time-period, however positive TUNEL staining was observed in ZnO NM treated tissues at day 14 which appeared to increase proportionally with increasing exposure concentration (Fig. 5). Increase in apoptotic cell death and reduction in TEER at day 14 suggests some degree of NM-mediated tissue degradation/damage occurred at 25 $\mu\text{g}/\text{cm}^2$ ZnO.

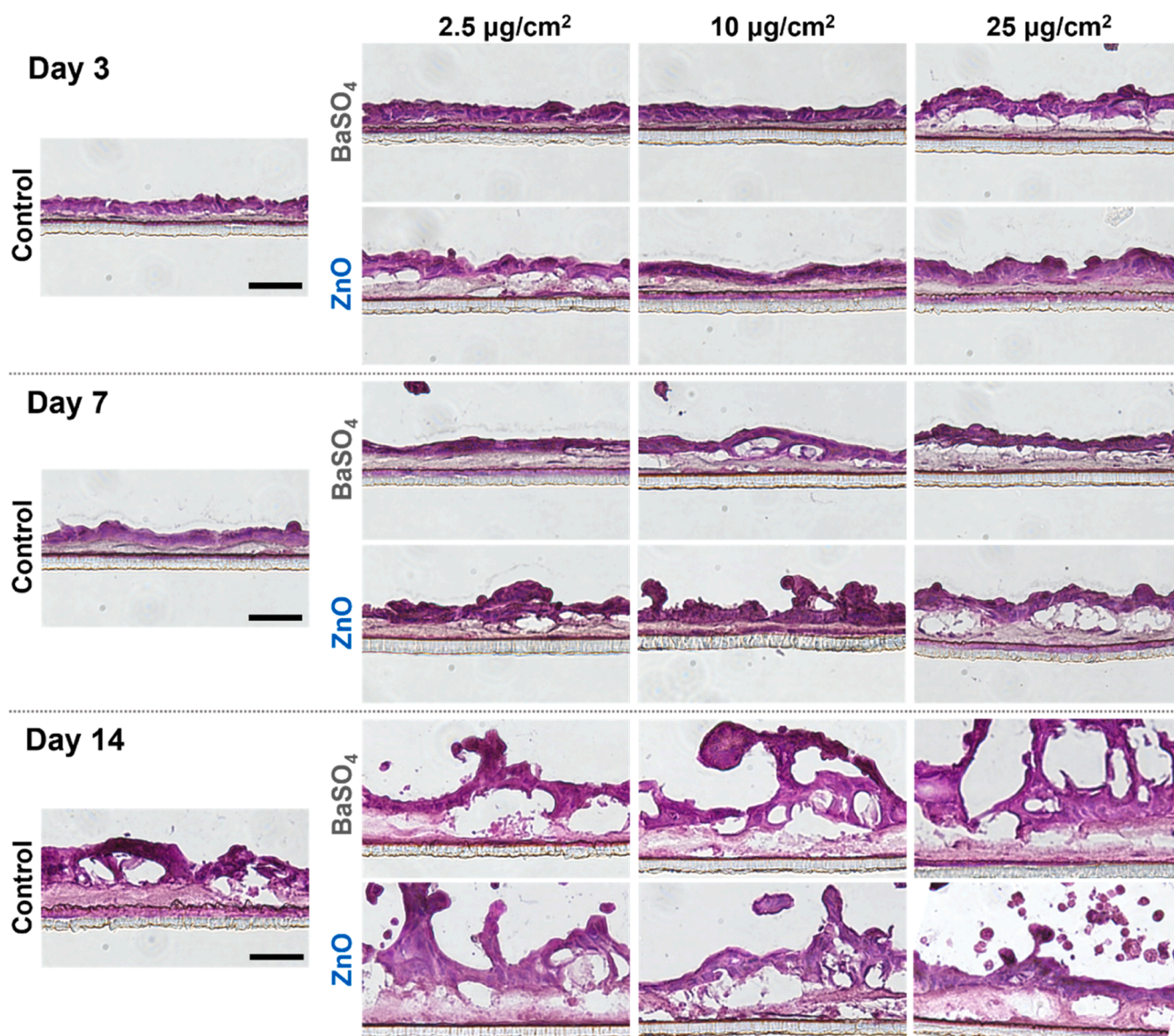


Fig. 3. Histological analysis (H&E staining) of the sectioned airway model exposed to various concentrations (2.5, 10, 25 $\mu\text{g}/\text{cm}^2$) NMs (ZnO and BaSO₄) for 3, 7, and 14 days (scale bar = 50 μm).

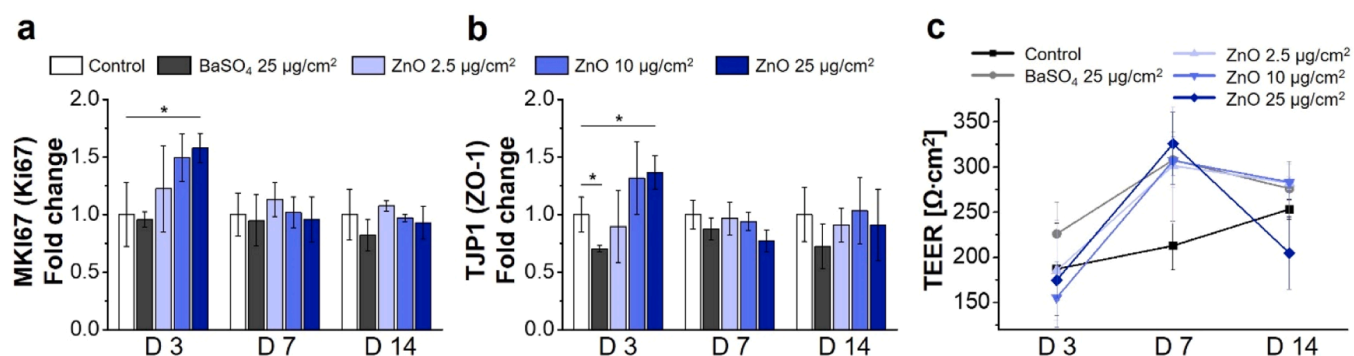


Fig. 4. Evaluation of tissue proliferation and cell junction in the airway model exposed to various concentrations of NMs (ZnO: 2.5, 10, 25 µg/cm² and BaSO₄: 25 µg/cm²) for 3, 7, and 14 days. a, b) Comparison of MKI67 (Ki67) and TJP1 (ZO-1) gene expression profiles (n = 3). The expression level of each gene was normalised by the expression level of the control group for each day. c) Comparison of trans-epithelial electrical resistance (TEER) to identify the tissue barrier integrity post exposure to NMs (n = 5).

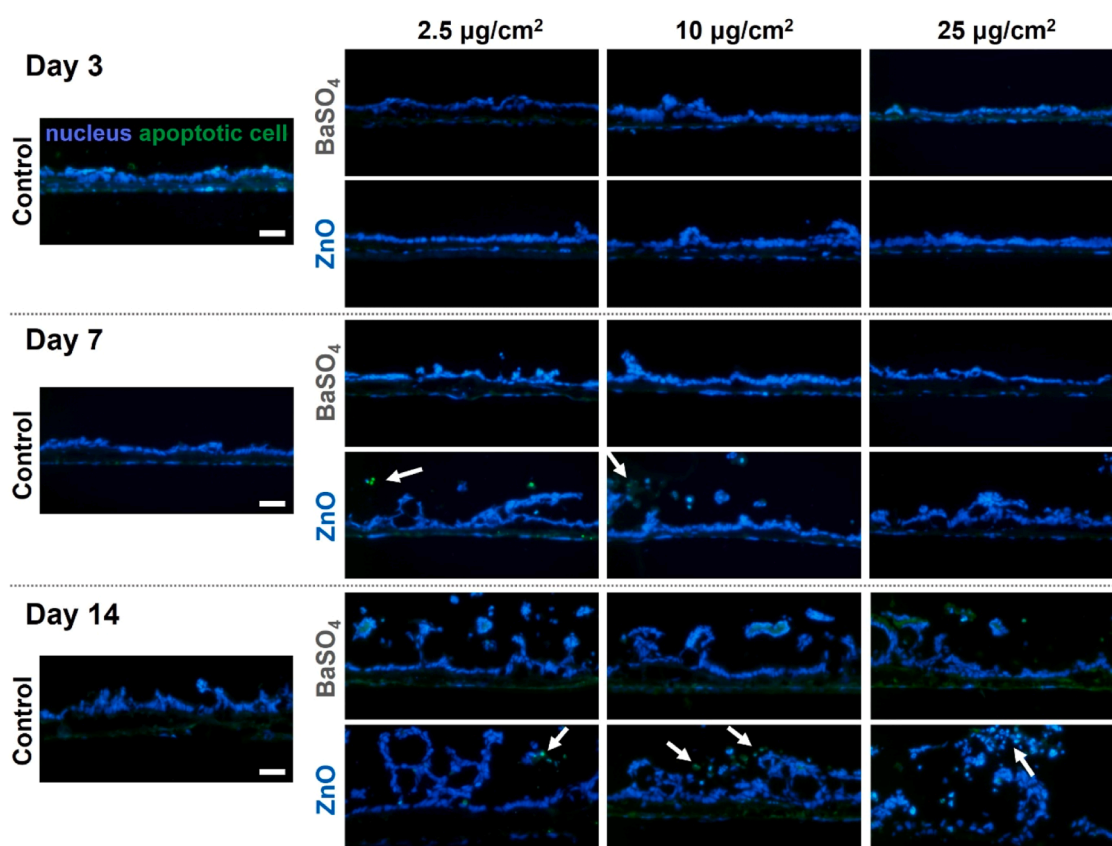


Fig. 5. Assessment of apoptotic cell death in the airway tissue constructs exposed to various concentrations (2.5, 10, 25 µg/cm²) of NMs (ZnO and BaSO₄) for 3, 7, and 14 days. TUNEL-stained apoptotic cells are shown in green and nuclei are shown in blue. Arrows indicate apoptotic cells (Scale bar = 50 µm).

Pro-inflammatory response changes induced by NM exposure

We next assessed whether exposure to ZnO NM and BaSO₄ NM induced pro-inflammatory responses in the airway tissue model by measuring changes in expression of key inflammation-mediating genes over time (Fig. 6 a-d). Significant dose-dependent and temporal changes were observed in response to ZnO NMs for a variety of the genes analysed, which suggests the initiation of a pro-inflammatory response in the airway tissue model, whereas the tissue response to BaSO₄ was weaker. After exposure to ZnO NM, an overall upregulation of pro-inflammatory gene expression was observed at day 3, followed by a significant decrease compared to control at day 7 before returning to

control levels for IL-1β and IL-8 at D14. VEGF expression remained depressed compared to control at day 14, potentially reflecting the regulation of a pro-inflammatory response through negative feedback mechanisms. On the other hand, the expression of SAA-1, an acute phase response protein, decreased significantly at day 7 but significantly increased (2-fold) in response to all doses of ZnO NMs at D14. A reversed pattern of decrease in SAA-1 expression was observed at D14 after BaSO₄ treatment.

Cytokine release into the basal compartment supernatant was measured by ELISA to evaluate the dose-dependent pro-inflammatory responses instigated by exposure to ZnO and BaSO₄ NM (Fig. 6 e-j). Specifically, an early and persistent increase in IL-6, IL-8 and TNFα

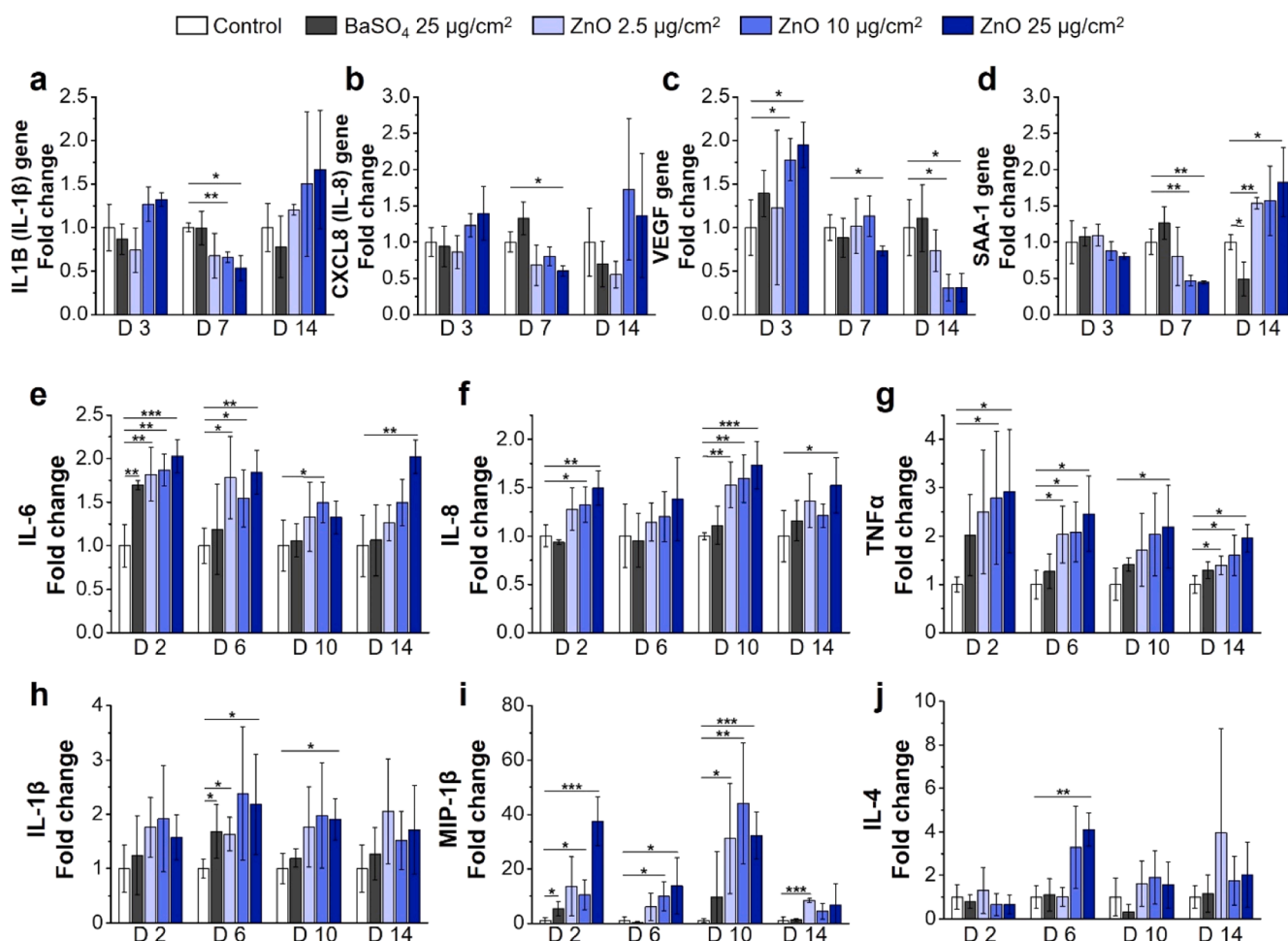


Fig. 6. Pro-inflammatory response changes in the airway model exposed to various concentrations of NMs (ZnO: 2.5, 10, 25 µg/cm² and BaSO₄: 25 µg/cm²) for 14 days. a-d) Comparative analysis of IL1B (IL-1β), CXCL8 (IL-8), VEGF, and SAA-1 gene expressions in the bioprinted airway tissue. e-j) Comparative analysis of IL-6, IL-8, TNFα, IL-1β, MIP-1β, and IL-4 cytokine release into the basal compartment. Expression levels were normalised by those of the control group for each day (n = 3). Significance levels were denoted as follows: * for p < 0.05, ** for p < 0.01, and *** for p < 0.001.

release was recorded whereas initial increases in IL-1β (D6 and D10) and MIP-1β (D2, D6, D10) declined by D14. An increase at D6 in IL-4 protein levels in response to 10 and 25 µg/cm² ZnO was similarly not maintained over time. Only minimal changes in cytokine levels were observed in response to BaSO₄.

The results present a dynamic profile of measurable pro-inflammatory changes triggered within the airway tissue model in response to ZnO NM. Taken together with the previously observed histological changes, evaluation of 3D bioprinted airway tissue models for NMs revealed differential responses between ZnO and BaSO₄ NMs when exposed to the same NM mass concentrations.

Comparison with Tier 1 assays

A number of Tier 1 hazard assessment assays, including acellular reactivity (Figs. S6) and 2D epithelial cell monocultures (Fig. 7, S7), were conducted for comparison with the airway tissue model and allow the potential added benefits of a proposed Tier 2 model to be evaluated. The aim of the study is to compare the bioprinted airway model with the standard Tier 1 methods used in the field in terms of what information can be derived from each model set up that will inform hazard assessment. Therefore, the Tier 1 assessment was conducted following standard high throughput assay protocols, as recommended in the nanotoxicology standard operating procedures and published Integrated Approaches to Testing and Assessment [4].

Acellular reactivity

Intrinsic ROS production was measured by DCFH₂-DA assay. Both ZnO NM and BaSO₄ NM were shown to produce relatively low levels of ROS in comparison to benchmark reactive CuO NM (Figure S6).

Exposure of 2D epithelial cell monocultures to NMs

Twenty-four hours after seeding, Calu-3 epithelial cells were exposed to ZnO and BaSO₄ NMs at comparable exposure concentrations used in the airway tissue model (2.5, 5, 25 µg/cm²) (Fig. 7a). Toxicity endpoints were measured after 24- and 72-hours exposure. Results showed a dose dependent decrease in cell viability was observed at 24 h after exposure to ZnO NM which increased in magnitude by 72 h (Fig. 7b). Calu-3 cells remained viable over the 72-h exposure to BaSO₄. As a control Calu-3 cells seeded directly onto the transwell membrane were exposed to ZnO and BaSO₄ and imaged by light microscopy after 24 hours. In line with the metabolic measure of cell viability, extensive cell loss was observed in ZnO-treated cells compared to BaSO₄ or untreated wells (Figure S7). A corresponding pattern of changes in cell metabolic activity was measured by Alamar Blue assay (Fig. 7c). Although an initial increase in intracellular ROS was observed in response to ZnO NM at 24 h, the highest concentration of ZnO (25 µg/cm²) caused a significant decrease in signal at 72 h, likely reflecting the significant loss of cell viability observed (Fig. 7d).

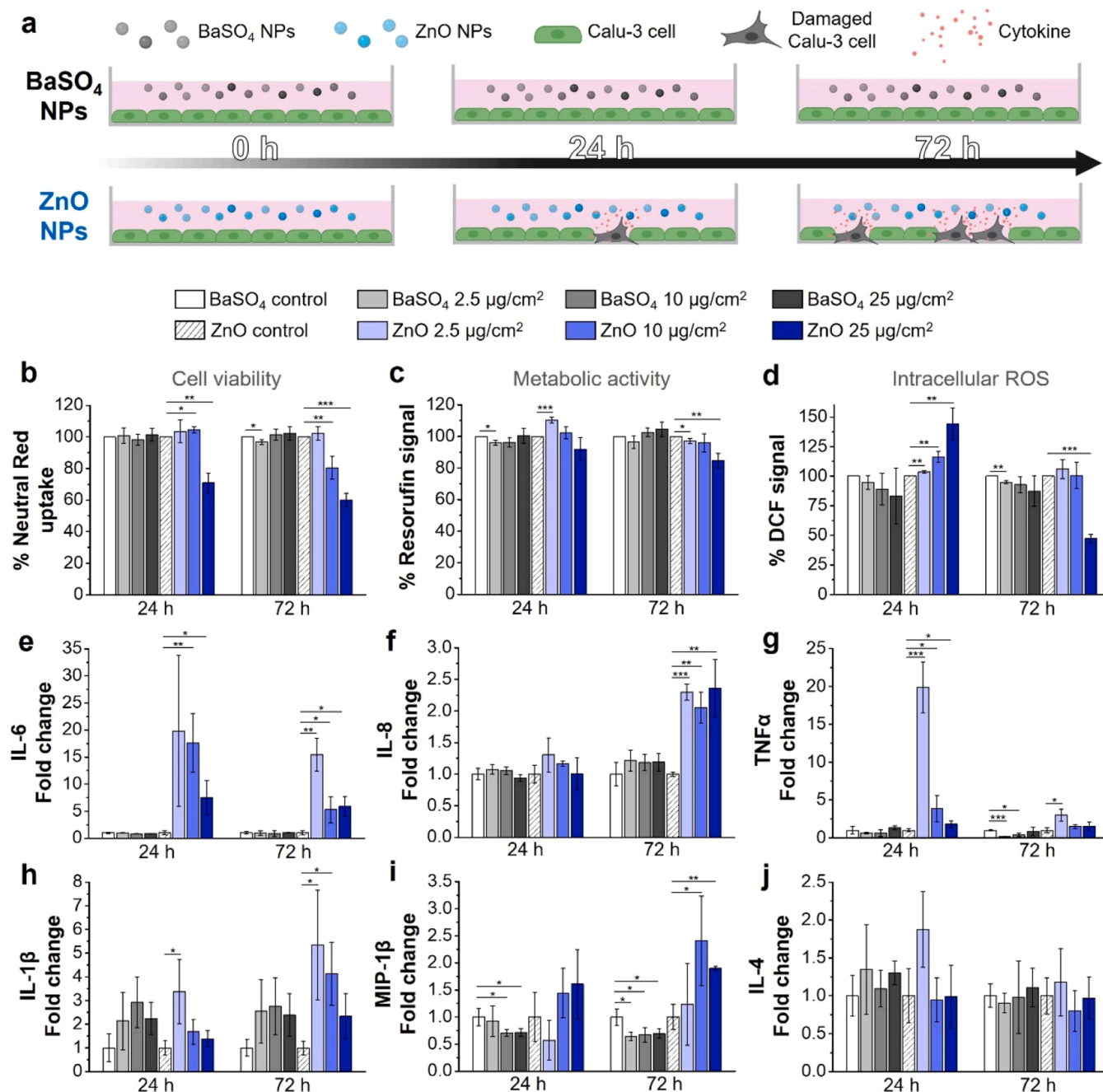


Fig. 7. Tier 1 hazard assessment of BaSO₄ and ZnO NM using Calu-3 2D cell monoculture. a) Schematic of experimental design. b) Cell viability as measured by Neutral red uptake after 24 h and 72 h exposure to 2.5, 10 or 25 $\mu\text{g}/\text{cm}^2$ of BaSO₄ or ZnO NM. c) Metabolic activity as measured by Alamar Blue assay (conversion of resazurin to resorufin) after 24 h and 72 h exposure to 2.5, 10 or 25 $\mu\text{g}/\text{cm}^2$ of BaSO₄ or ZnO NM. d) Intracellular ROS production as measured by DCFH₂-DA probe after 24 h and 72 h exposure to 2.5, 10 or 25 $\mu\text{g}/\text{cm}^2$ of BaSO₄ or ZnO NM. b-d) Data normalised to untreated control (n = 3). e-j) Fold change in release of cytokine panel as compared to untreated control. Cytokine release measured by ELISA assay. (n = 3). Statistical significance was assessed by a two-tailed *t*-test, treatment versus control. Significance levels were denoted as follows: * for $p < 0.05$, ** for $p < 0.01$, and *** for $p < 0.001$.

Cytokine release measured by ELISA was used as an indicator of pro-inflammatory response changes. Low dose ZnO (2.5 $\mu\text{g}/\text{cm}^2$) induced a significant increase in IL-1 β , IL-6 and TNF α release at 24 h which was sustained over the 3-day. An inverse dose-dependent relationship was observed for these cytokines both after 24 and 72 h which again can most likely be explained by the loss of cell viability at higher ZnO NM exposures. Interestingly, a delayed induction of both IL-8 and MIP-1 β chemokines was observed in response to the higher doses of ZnO (10 $\mu\text{g}/\text{cm}^2$, 25 $\mu\text{g}/\text{cm}^2$). No significant increase in cytokine release was measured in response to BaSO₄, however a significant suppression of MIP-1 β release was observed after both 24- and 72-h exposures. These

results highlight the differential acute responses of airway epithelial cell monocultures to direct exposure to ZnO and BaSO₄ NMs.

Comparison of Tier 1 and Tier 2 assay hazard assessment

Table S4 summarizes the responses of each Tier 1 (acellular reactivity and Calu-3 2D cell monoculture) and the proposed Tier 2 (printed airway tissue model to ZnO and BaSO₄ NMs). It is worth highlighting Tier 1 assays were conducted according to status quo in the field. Tier 1 models are designed to be low cost and high throughput; the standard Tier 1 approach is to use 96-well plates to culture cells

submerged in media for rapid screening assays. The airway tissue model described here was not designed as a progression of the simple Tier 1 models and therefore the models used at each Tier are not directly comparable. Deeper understanding of the superiority of the airway model over simple monocultures of cells at a mechanistic level would be better served by direct comparison of models with minimal differences in model set-up and therefore will be the focus of future studies. Both Tier 1 and Tier 2 models successfully differentiated the high toxicity ZnO NM from low toxicity BaSO₄ although key differences between model sensitivity were observed. Acute cytotoxicity to ZnO NMs was measured in Calu-3 monoculture starting at 24 h whereas apoptotic cells in the Calu-3 cells of the airway tissue model appeared only at D14 post exposure. The acute sensitivity of Calu-3 cells to ZnO exposure observed in the Tier 1 assay did not appear to be due to the cell culture conditions (96-well format) as a high degree of cell loss and disruption of epithelial barrier is observed in Calu-3 cells cultured directly on Transwell inserts (Figure S7). Furthermore, although both models demonstrated an acute and persistent induction of inflammatory cytokine release, inflammatory response of Calu-3 2D cell monoculture was induced by the lowest exposure concentrations whereas higher exposure concentrations were required to stimulate release of measurable levels of cytokine release in the airway tissue model. These discrepancies could be reflective of the impact of the tissue microstructure on Calu-3 sensitivity to ZnO NMs. Previous studies have identified greater resistance of Calu-3 cells to toxic insult when cultured in co-culture models at the ALI compared to monocultures consistent with the results presented here [26]. Similarly, Muller et al. [27] have previously presented an alternative immune response to NMs when triple cell co-cultures consisting of A549 human epithelial lung cells, human monocyte-derived macrophages and monocyte-derived dendritic cells exposed to combustion-derived NPs (diesel exhaust particles) and to manufactured NPs (titanium dioxide and single-walled carbon nanotubes) were compared to single cell cultures. Interestingly, responses in the triple cell co-culture showed decreased total antioxidant capacity and IL-8 concentrations whereas the TNF α concentrations were higher than the expected values calculated from the monocultures. The interplay of different lung cell types therefore substantially modulates the oxidative stress and the inflammatory responses after NP exposure, highlighting the additional information obtained from more complex models. The sensitivity of the single cell culture to short term exposure limits the potential to use such models to study the mechanism of hazard or more subtle immunomodulatory effects of ZnO NM exposure. The bioprinted airway model could therefore provide more in-depth information on the hazard posed by NM exposure going beyond blunt cytotoxicity and provide information on immunoactivation over time which may better replicate the inflammatory response seen after *in vivo* exposures [28]. The ability of the airway model to differentiate known high and low toxicity NM demonstrated here opens the potential to use this model for deeper mechanistic studies to further biological consequences of NM toxicity, with oxidative stress responses and genotoxicity priority endpoints for further analysis. The extended longevity offered by the bioprinted airway model also presents the opportunity for repeat low dose exposures which more realistically replicate human exposures. Currently, this is not commonplace within *in vitro* lung cell cultures where the majority of studies have been conducted within very limited timeframes of up to 72 h even when more complex models have been employed [29, 30].

Comparison of Tier 2 bioprinted airway model and Tier 3 *in vivo* hazard assessment

Physiological relevance of an *in vitro* model should be demonstrated by the ability of the model to respond to toxic insult in a manner which replicates pathological changes observed *in vivo* (Table S5). Table 1 outlines how the responses of the 3D bioprinted airway model to ZnO NM align with or predict the pathological changes consistently

Table 1

Comparison of responses to ZnO exposure observed *in vivo* [31–36] and 3D bioprinted airway model.

<i>In vivo</i> pathological changes	Bioprinted 3D airway tissue model responses
Alveolar tissue disruption and loss of barrier integrity	Apoptosis and reduction in TEER at D14 in high dose ZnO
Epithelial cell desquamation	Delamination of Calu-3 lung epithelial layer
Epithelial cell hyperplasia	Upregulation of Ki67 gene expression and increased thickening of cell layers seen in histology
Acute inflammation mediated by upregulation of cytokines	Increased pro-inflammatory gene expression and IL-1 β , IL-6 and TNF α release measured by ELISA
Influx of inflammatory cells	Increase in IL-8 neutrophil chemokine, MIP-1 β monocyte chemokine release

identified in previous *in vivo* studies.

Pathological response to ZnO NMs exposure is associated with a defined mechanism of toxicity dependent on the dissolution of ZnO to reactive Zn²⁺ in the biological milieu of the lungs and subsequent increase of ROS leading to tissue damage, oxidative stress and acute inflammation [37]. Human studies have confirmed inhalation to zinc oxide fumes causes metal fume fever, an occupational flu-like illness [38]. This self-limited febrile syndrome, which is common among welders, is characterised by constitutional symptoms and an associated pulmonary inflammatory cellular response. Concentration-dependent increases in acute phase proteins (CRP and SAA) and neutrophils in blood were detected after ZnO inhalation [39]. *In vitro* and *in vivo* studies have consistently reported acute cytotoxicity and inflammatory response to ZnO NM exposure [20]. Many of the same biomarkers correspond to the drivers of metal fume fever providing useful criteria to benchmark against when considering how best to evaluate an alternative model as appropriate to predict human-relevant hazard. The potential for ZnO NM to induce metal fume fever is similarly predicted from the hazard responses reported here.

BaSO₄ generally considered to be relatively inert and has previously been classified as a ‘passive’ NM by [20] based on adherence to the following criteria: Toxic component (element or molecule) < 0.1 %; surface reactivity: < 10 % of Mn₂O₃ reactivity in FRAS or cytochrome C assays; no cellular effects at 610 $\mu\text{g}/\text{cm}^2$; confirmatory threshold value in respect to low toxic potency, i.e., NOAEC in short-term inhalation study (STIS) > 10 mg/m^3 . The lack of sustained toxic response reported here adds further weight to the classification of BaSO₄ as a relatively low toxicity NM. Although it should be recognised that *in vitro* models may not be appropriate to detect the potential to discount the well-recognised hazard posed by retention and build-up of poorly soluble, low-toxicity particles [40].

In summary, here we reported measurable pro-inflammatory and cytotoxic responses triggered in the 3D bioprinted airway tissue model after exposure to ZnO and to a lesser extent BaSO₄. The data provided confirms the ability of this model to differentiate between high and low reactivity NMs based on the assessment of endpoints highly relevant to potential hazard linked to human exposure to inhaled toxins. Further testing of the bioprinted airway model with other forms of NMs which may cause toxicity via broader or alternative mechanisms of action will be an interesting avenue for future work.

Comparison of 3D bioprinted airway tissue model with state-of-the-science alternative models

According to Nossa et al. [10], the specifications for an ideal “physiologically relevant” engineered human *in vitro* alveolus/airway model include the use of human-derived cells that compose the native alveolar barrier and consist of a layer of simple squamous epithelium; a layer of endothelial cells of the capillary wall; and the basement membrane between the two. The model should be amenable to the culture of

cells at the ALI to mimic the *in vivo* microenvironment where the epithelial lung cells are in contact with humid air on one side and blood on the other and incorporate substrate for growing cells with properties similar to native tissue in terms of chemical composition and biomechanical behaviour. Additional advantageous mechanical features would be a fluidic system that reproduces the blood flow through the alveolar capillaries to provide adequate oxygenation and nutrients to the cell, as well as physiological shear stress to endothelial cells, and the ability to subject the substrate to mechanical cyclic stretching to reproduce alveolar barrier motion during breathing.

Our 3D bioprinted airway model used in this study adheres to three of the suggested criteria, lacking only the dynamic features of fluid flow. No other model identified currently incorporated all features with only a small number including the mechanosignalling provided by a relevant substrate (mimicking the ECM/basement membrane), shear stress from fluid flow or cyclical stretching. Importantly the bioprinting approach utilised here led to the consistent construction of airway barrier model with unprecedented thinness and more physiologically relevant degree of contact between epithelial/endothelial cells compared to other multicell models as our model is not based on the growth of each cell type on opposite sides of a $\sim > 10\mu\text{m}$ thick polycarbonate or polyester porous membrane.

Direct comparison with other available complex airway tissue models cannot be conducted as no other model identified has examined the responses to the same NMs (NM110 and NM220) under investigation here. However, a review of the alternative complex *in vitro* respiratory tissue models which have been more broadly used in NM hazard studies was conducted to identify the key common features, and relative strengths and weaknesses of each approach.

For inclusion in this review, a 'complex *in vitro* airway tissue model' was required to include at least three relevant cell types and have been used in a study specifically assessing the toxicity of NMs. The conclusions of this state-of-the-science are summarised in Table 2 (Full details in Table S6). Regarding the construction of the different models, although all models incorporate a combination of multiple relevant lung cell lines differences in cell selection exist with some approaches focusing on the combination of epithelial and immune cells whereas other approaches prioritize the inclusion of lung epithelial and structural stromal cells including fibroblasts and endothelial cells. Few models include an ECM component and no other model reported to date constructs their model using precise and highly controlled bioprinting techniques highlighting the advantages of the model constructed here.

The common objective of each study reviewed is the application of these models for NM hazard assessment. No single material has been used across studies to test different model set-ups so direct comparison of the application of the models for hazard assessment cannot be conducted. Most studies have selected endpoints which account for the known mechanisms of toxicity of particles and key events involved in the pathogenesis of lung disease such as cytotoxicity, barrier integrity, pro-inflammatory changes, oxidative stress and genotoxicity or DNA damage and the majority of studies focused on measuring the acute toxicity of particles at 24–72 h time points post exposure. In contrast, we present a longer-term assessment of hazard up to 14 days-post exposure demonstrating both the longevity of the airway tissue model over time and revealing the progressive adverse response to exposure to ZnO NMs.

Internal comparison with simpler systems as conducted here largely show the ability of the models to identify acute hazard, however, no consistent trend of increased or decreased sensitivity of the wider panel of complex tissue models to particle exposure compared to simple systems was observed. Although most studies have not directly compared their models to existing or *de novo* data reporting the *in vivo* toxicity of the identical source material, similar pathological changes were regularly noted *in vivo* to similar substances i.e., different forms of NMs with the same composition. Here, we specifically selected well-characterised case study materials with extensive existing *in vivo* toxicity data to allow direct comparison and therefore provided robust evidence to support the

Table 2

Conclusions on state-of-science review. Summary of key common features, and relative strengths and weaknesses of the alternative complex *in vitro* respiratory tissue models used for NM hazard assessment.

Cell types	<ul style="list-style-type: none"> - Majority of models rely on cell lines - Variety of cell types included in models - Most common combinations include epithelial cells, fibroblasts and macrophages
Extracellular matrix Model set-up	<ul style="list-style-type: none"> - Majority of models do not include ECM - Majority of models co-culture cells supported by cell culture insert - Majority of models culture epithelial cells at ALI - Exposure via cloud system is commonly used - Recent focus on incorporation of dynamic flow
Particle treatment Timeframe	<ul style="list-style-type: none"> - Wide variety of particle types have been tested - Majority of studies report acute 24–48 h exposures. - Few models report repeat exposures or longer-term responses
Endpoints assessed	<ul style="list-style-type: none"> - Majority of studies report common toxicity endpoints of cytotoxicity, cell viability/metabolic activity, pro-inflammatory cytokine release, TEER and barrier integrity, oxidative stress and genotoxicity
Comparison to simple <i>in vitro</i>	<ul style="list-style-type: none"> - Majority of studies include direct comparison to simpler models such as 2D cell monoculture - No consistent trend of increased or decreased sensitivity of complex models to particle exposure compared to simple system
Predictivity of <i>in vivo</i> response	<ul style="list-style-type: none"> - Few studies report direct comparison to <i>in vivo</i> responses to the same material - Some studies refer directly to <i>in vivo</i> responses elicited by the same test materials - Most studies refer to <i>in vivo</i> responses to similar test materials e.g., same chemical composition reported in the literature - Most models replicate some pathological changes observed <i>in vivo</i> however evidence of increased predictivity over simple system or increased physiological relevance of complex model remains limited
Transferability	<ul style="list-style-type: none"> - Most models are reliant on widely available reagents such as commercially available cell lines and Transwell inserts - Some models require specialized equipment and technical expertise - Few models have been tested in intralaboratory comparison

predictivity of our model.

We consider the incorporation of the ECM in a multicell model to better replicate the lung airway tissue as a major benefit of the model presented here (Table 3). From our review of the literature the majority of other complex *in vitro* models do not contain an ECM component, with cells directly grown on tissue culture plastics and synthetic polymer membrane inserts. The ECM of the lungs is composed of a complex 3D network of proteins, glycoproteins, and polysaccharides. Once regarded as a predominantly structural framework, it is now well recognised that the ECM incorporates a diverse array of bioactive molecules with important functional roles [41]. Cell-ECM interactions can direct cell survival, adhesion, migration, proliferation, and differentiation. Collagen, which constitutes the main structural element of the ECM of the lung [42], providing tensile strength, regulating cell adhesion,

Table 3

Strengths and limitations of bioprinted lung tissue model.

Strengths of bioprinted lung tissue model	Limitations of bioprinted lung tissue model
<ul style="list-style-type: none"> - Incorporation of ECM - Longer-term responses measured compared to 2D cell monoculture - Validated with well-characterised, hazard data-rich test materials 	<ul style="list-style-type: none"> - Technical challenges of bioprinting - Transferability needs to be demonstrated - Lack of immune cell limits physiological relevance

supporting chemotaxis and migration, and directing tissue development [43], was included in this model to account for the potential influence of the ECM-cell signalling on lung epithelial cell sensitivity to toxic insult. Although there are some examples of alternative models which have coated tissue culture plastic with biomimetic ECM components as far as we are aware this is the first example of an artificially constructed airway tissue model used in NM hazard assessment which utilised the ECM component to perform as a tissue scaffold supporting the growth of interstitial fibroblasts as occurs naturally in the lung tissue.

Inclusion of different cell types allows for the primary response to direct interaction with NMs to be detected in the epithelial cell layer as well as potential secondary effects due to cell-cell interactions to be assessed overtime. Fibroblasts were included in the collagen matrix as the major producers of collagen and play an active role in the dynamic organization of collagen network structures. The inclusion of fibroblasts could therefore support the integrity and longevity of the artificial airway model. Activation of fibroblasts to myofibroblast, key players in the development of pulmonary fibrosis can propagate the inflammatory response; fibroblast activation may occur through direct interaction with toxic substances or alternatively in response to signals released by other cells influencing the tissue microenvironment [44,45]. An exciting future application of this model will be to study the mechanisms of particle-induced pulmonary fibrosis development, as changes in structural deposition, pulmonary function, epithelial-mesenchymal transition, and fibrosis markers were already observed in response to treating the 3D airway barrier model with pro-fibrotic cytokine in an induced fibrosis model used as a novel testing platform and disease model to evaluate potential anti-fibrotic drug efficacy [18].

Endothelial cells are also included in this model to complete the tissue complement of the airway-blood barrier. The focus of this study was on the tissue level changes observed after exposure to NMs therefore specific responses could not be directly assigned to individual cell types. Interestingly we observed upregulation of SAA-1 after exposure to ZnO NM which is marker of metal fume fever and has a role in the development of cardiovascular disease [46]. It will therefore be interesting to examine in more detail the potential impact of increased SAA-1 on the endothelial cell compartment.

In terms of physiological relevance, the lack of immune cells e.g., macrophages and/or dendritic cells, which have been widely included in alternative complex models, may be seen as a significant limitation of the bioprinted airway model for the hazard assessment of NMs. Given the known importance of the macrophages as a primary defence mechanism against inhaled foreign substances which directly interact with inhaled substances and propagate the subsequent inflammatory response [47], the full picture of NM toxicity may not be represented by the responses observed here. However, as the majority of inhaled NMs will deposit on the epithelial cell layer of the lungs unpicking the toxic response of the epithelial cells is crucial. Indeed, here we observe changes indicative of the *in vivo* response to ZnO NM were identified without the inclusion of macrophages suggesting an important role played by lung epithelial cells in sensing and responding to inhaled toxins.

Transferability is key to the wider adoption and route to validation of novel alternative models. Two primary limitations which may present a barrier to wider adoption of the bioprinted airway model have been identified which included the potential technical challenges of bioprinting and need for technical expertise and specialist equipment. An interlaboratory comparison study will need to be taken to evaluate the transferability of the model presented here to other labs and consistency in hazard results demonstrated to promote the wider use of this model for regulatory hazard assessment and build the confidence required to support the mutual acceptance of data.

Other alternative complex model systems which do not use bioprinted materials may have lower barriers to wider adoption but at the expense of other aspects of physiological relevance. Increasing recognition of the need to include mechanical components such as the

incorporation of microfluidics to mimic blood flow and mechanical stress to replicate the breathing action of the lung, to continue to build physiological relevance, emphasizes the need for an interdisciplinary approach to model design and application to prevent the additional technical requirements of these models acting as barriers to wider adoption in future.

For many NMs, and especially for novel ones, hazards are largely unknown, and cannot be predicted only based on physicochemical (PC) characterisation. Therefore, carrying out suitable hazard testing at the early stages of product development is of utmost importance to support the sustainable growth of this key strategic industry. Innovative Tier 2 assays, such as the model presented here, may be more predictive option to support SbD than Tier 1 assays due to a higher physiological relevance, or by allowing identification of the mechanism triggering toxicity, however all complex *in vitro* models proposed to fill the Tier 2 level of testing currently lack standardisation. Tier 3 *in vivo* studies are likely required for the foreseeable future to provide the necessary data on NM distribution and fate and to identify systemic effects, especially for regulatory risk assessment. However, integration of sophisticated *in vitro* airway models in with newly generated 'smart' *in vivo* models such as toxicity reporter mice could lead to the development of next generation tiered testing strategies which further refine and streamline the hazard assessment process.

A set of performance criteria has been proposed to evaluate the suitability of *in vitro* methods for hazard assessment of NMs for the purpose of SbD [14]. Criteria were primarily designed to be appropriate to assess the performance and state of readiness of endpoint measurement assays however a number of the criteria could similarly be applied to the evaluation of novel *in vitro* models, such as predictivity of *in vivo* responses. Prediction accuracy of a model is considered a function of specificity, ability to detect true negatives (BaSO₄) and sensitivity, ability to detect true positives (ZnO) which we have confirmed for the bioprinted airway model in the data reported here. It is important to highlight that correlation of *in vitro* effects to *in vivo* potency is not possible due to the simplicity of the endpoints measured. Correlation is not a requirement of SbD but rather the emphasis should be placed on the ability of a model or assay to detect potentially hazardous materials by their ability to trigger known mechanisms of toxicity. For SbD purposes a model should be robust and reliable; consistency in model construction is provided here through use of bioprinting technology to mitigate variance inherent in manual pipetting of cell layers. Furthermore, the model must be compatible for use with NMs. We demonstrated the use of the bioprinted tissue model exposed to NMs under pseudo-ALI conditions to more accurately represent inhalation exposure compared to the use of submerged cell culture, but full ALI could as readily be employed with the appropriate aerosolization equipment. The bioprinted airway model therefore meets many of the criteria for appropriate use to support SbD decision making.

Conclusion

In this study, we evaluated the application of a 3D bioprinted lung tissue model in a first-in-kind approach to the inhalation hazard assessment of NMs, which was achieved by using the model to assess the toxicity of two case study NMs, characterised as highly reactive (ZnO NM-110) or passive (BaSO₄ NM-220) in previous *in vitro* and *in vivo* hazard assessment studies. The responses of the bioprinted model were contextualised with reference to simple Tier 1 epithelial cell monoculture exposures, hazard responses identified *in vivo* and in human exposures. Evidence was provided to support the further development of this model to, address a significant gap in our current toolbox for NM toxicity testing, which may have direct utility for SbD purposes. Application of stable, tightly controlled airway models for studying fundamental cell-cell and cell-matrix interactions in response to inhaled toxins which are amenable to manipulation offer the exciting potential to design mechanistic studies to better understand the complex

intracellular interactions which take place at the tissue level in the pathogenesis of particle-related lung disease. In parallel appraisal of the model limitations allowed the critical requirements which may be required for further validation of the model to be recognised. Addressing these barriers to wider adoption may pave the way for validation of this model for regulatory purposes.

CRedit authorship contribution statement

Lee Yunji: Writing – review & editing, Writing – original draft, Visualization, Investigation, Formal analysis, Data curation, Conceptualization. **McAllister Katie:** Writing – review & editing, Visualization, Investigation, Formal analysis, Data curation. **Lee Hwa-Rim:** Writing – review & editing, Writing – original draft, Visualization, Supervision, Formal analysis, Data curation, Conceptualization. **Jung Sungjune:** Writing – review & editing, Writing – original draft, Supervision, Project administration, Funding acquisition, Conceptualization. **Murphy Fiona:** Writing – review & editing, Writing – original draft, Visualization, Supervision, Project administration, Investigation, Funding acquisition, Formal analysis, Data curation, Conceptualization.

Declaration of Competing Interest

The authors declare that they have no known competing financial interests or personal relationships that could have appeared to influence the work reported in this paper.

Acknowledgements

This study was supported by the Royal Society of Edinburgh SAPHIRE fund (2895) and the National Research Foundation of Korea Grants (NRF-2022R1A2C2012272).

Appendix A. Supporting information

Supplementary data associated with this article can be found in the online version at [doi:10.1016/j.nantod.2025.102655](https://doi.org/10.1016/j.nantod.2025.102655).

Data availability

Data will be made available on request.

References

- M.J. Moné, et al., Setting the stage for next-generation risk assessment with non-animal approaches: the EU-ToxRisk project experience (in eng), *Arch. Toxicol.* 94 (10) (Oct 2020) 3581–3592, <https://doi.org/10.1007/s00204-020-02866-4>.
- I. Fischer, C. Milton, H. Wallace, Toxicity testing is evolving!, *Toxicol. Res.* 9 (2) (2020) 67–80, <https://doi.org/10.1093/toxres/taaa011>.
- F. Murphy, et al., An integrated approach to testing and assessment of high aspect ratio nanomaterials and its application for grouping based on a common mesothelioma hazard, /04/01/ 2021, *NanoImpact* 22 (2021) 100314, <https://doi.org/10.1016/j.impact.2021.100314>.
- H.M. Braakhuis, et al., An integrated approach to testing and assessment to support grouping and read-across of nanomaterials after inhalation exposure (in eng), *Appl. Vitro. Toxicol.* 7 (3) (Sep 1 2021) 112–128, <https://doi.org/10.1089/aivt.2021.0009>.
- F. Murphy, et al., Grouping MWCNTs based on their similar potential to cause pulmonary hazard after inhalation: a case-study (in eng), *Part Fibre Toxicol.* 19 (1) (Jul 20 2022) 50, <https://doi.org/10.1186/s12989-022-00487-6>.
- S.A. Langhans, Three-dimensional in vitro cell culture models in drug discovery and drug repositioning (in English), *Front. Pharmacol.* 9 (2018-January-23 2018), <https://doi.org/10.3389/fphar.2018.00006>.
- M. Shamseddin, J. Obacz, M.J. Garnett, R.C. Rintoul, H.E. Francies, S.J. Marciniak, Use of preclinical models for malignant pleural mesothelioma, *Thorax* 76 (11) (2021) 1154, <https://doi.org/10.1136/thoraxjnl-2020-216602>.
- J.K. Burgess, T. Mauad, G. Tjin, J.C. Karlsson, G. Westergren-Thorsson, The extracellular matrix - the under-recognized element in lung disease (in eng), *J. Pathol.* 240 (4) (Dec 2016) 397–409, <https://doi.org/10.1002/path.4808>.
- T. Yanagihara, S.G. Chong, M. Vierhout, J.A. Hirota, K. Ask, M. Kolb, Current models of pulmonary fibrosis for future drug discovery efforts (in eng), *Expert Opin. Drug Discov.* 15 (8) (Aug 2020) 931–941, <https://doi.org/10.1080/17460441.2020.1755252>.
- R. Nossa, J. Costa, L. Cacopardo, A. Ahluwalia, Breathing in vitro: designs and applications of engineered lung models (in eng), *J. Tissue Eng.* 12 (Jan-Dec 2021), <https://doi.org/10.1177/20417314211008696>.
- E. Commission, et al., NANoREG framework for the safety assessment of nanomaterials, Publications Office of the European Union, 2017.
- A. Kraegeloh, B. Suarez-Merino, T. Sluijters, C. Micheletti, Implementation of safe-by-design for nanomaterial development and safe innovation: why we need a comprehensive approach (in eng), *Nanomaterials* 8 (4) (Apr 14 2018), <https://doi.org/10.3390/nano8040239>.
- D. Kang, et al., All-inkjet-printed 3D alveolar barrier model with physiologically relevant microarchitecture, *Adv. Sci.* 8 (10) (2021) 2004990, <https://doi.org/10.1002/advsc.202004990>.
- N. Ruijter, et al., The state of the art and challenges of in vitro methods for human hazard assessment of nanomaterials in the context of safe-by-design, *Nanomaterials* 13 (3) (2023) 472. (<https://www.mdpi.com/2079-4991/13/3/472>) ([Online]. Available:).
- S. Chai, et al., Dynamic monitoring of a 3D-printed airway tissue model using an organic electrochemical transistor, Art no. 122806, *Biomaterials* 314 (2025), <https://doi.org/10.1016/j.biomaterials.2024.122806>.
- Y. Lee, M.K. Lee, H.-R. Lee, B. Kim, M. Kim, S. Jung, 3D-printed airway model as a platform for SARS-CoV-2 infection and antiviral drug testing, /12/01/ 2024, *Biomaterials* 311 (2024) 122689, <https://doi.org/10.1016/j.biomaterials.2024.122689>.
- D. Kang, H. Lee, and S. Jung, "Use of a 3D Inkjet-Printed Model to Access Dust Particle Toxicology in the Human Alveolar Barrier," 2022.
- D. Kang, Y. Lee, W. Kim, H.-R. Lee, S. Jung, 3D pulmonary fibrosis model for anti-fibrotic drug discovery by inkjet-bioprinting, /12/23 2023, *Biomed. Mater.* 18 (1) (2022) 015024, <https://doi.org/10.1088/1748-605X/aca8e3>.
- N. Jeliazkova, et al., The eNanoMapper database for nanomaterial safety information (in eng), *Beilstein J. Nanotechnol.* 6 (2015) 1609–1634, <https://doi.org/10.3762/bjnano.6.165>.
- J.H.E. Arts, et al., Case studies putting the decision-making framework for the grouping and testing of nanomaterials (DF4nanoGrouping) into practice, /04/01/ 2016, *Regul. Toxicol. Pharmacol.* 76 (2016) 234–261, <https://doi.org/10.1016/j.yrtph.2015.11.020>.
- D. Schwotzer, et al., Effects from a 90-day inhalation toxicity study with cerium oxide and barium sulfate nanoparticles in rats, /07/12 2017, *Part. Fibre Toxicol.* 14 (1) (2017) 23, <https://doi.org/10.1186/s12989-017-0204-6>.
- N. Hadrup, et al., Acute phase response and inflammation following pulmonary exposure to low doses of zinc oxide nanoparticles in mice, /10/21 2019, *Nanotoxicology* 13 (9) (2019) 1275–1292, <https://doi.org/10.1080/17435390.2019.1654004>.
- S. Hankin, D. Boraschi, A. Duschl, C.-M. Lehr, H. Lichtenbeld, Towards nanotechnology regulation – publish the unpublishable, /06/01/ 2011, *Nano Today* 6 (3) (2011) 228–231, <https://doi.org/10.1016/j.nantod.2011.03.002>.
- V. Stone, et al., A framework for grouping and read-across of nanomaterials-supporting innovation and risk assessment, *Nano Today* 35 (2020) 100941.
- A. Haase, et al., Genotoxicity testing of different surface-functionalized SiO₂, ZrO₂ and silver nanomaterials in 3D human bronchial models, /12/01 2017, *Arch. Toxicol.* 91 (12) (2017) 3991–4007, <https://doi.org/10.1007/s00204-017-2015-9>.
- S. Chortarea, et al., Repeated exposure to carbon nanotube-based aerosols does not affect the functional properties of a 3D human epithelial airway model, /11/17 2015, *Nanotoxicology* 9 (8) (2015) 983–993, <https://doi.org/10.3109/17435390.2014.993344>.
- L. Müller, M. Riediker, P. Wick, M. Mohr, P. Gehr, B. Rothen-Rutishauser, Oxidative stress and inflammation response after nanoparticle exposure: differences between human lung cell monocultures and an advanced three-dimensional model of the human epithelial airways (doi: doi:), *J. R. Soc. Interface* 7 (1) (2010) S27–S40, <https://doi.org/10.1098/rsif.2009.0161.focus>.
- S. Hofer, N. Hofstätter, B. Punz, I. Hasenkopf, L. Johnson, M. Himly, Immunotoxicity of nanomaterials in health and disease: current challenges and emerging approaches for identifying immune modifiers in susceptible populations, *WIREs Nanomed. Nanobiotechnol.* 14 (6) (2022) e1804, <https://doi.org/10.1002/wnan.1804>.
- K. Meldrum, S.J. Evans, U. Vogel, L. Tran, S.H. Doak, M.J.D. Clift, The influence of exposure approaches to in vitro lung epithelial barrier models to assess engineered nanomaterial hazard, /01/02 2022, *Nanotoxicology* 16 (1) (2022) 114–134, <https://doi.org/10.1080/17435390.2022.2051627>.
- S. Chortarea, H. Barosova, M.J.D. Clift, P. Wick, A. Petri-Fink, B. Rothen-Rutishauser, Human asthmatic bronchial cells are more susceptible to subchronic repeated exposures of aerosolized carbon nanotubes at occupationally relevant doses than healthy cells, /08/22 2017, *ACS Nano* 11 (8) (2017) 7615–7625, <https://doi.org/10.1021/acsnano.7b01992>.
- C.L. Klein, K. Wiench, M. Wiemann, L. Ma-Hock, B. van Ravenzwaay, R. Landsiedel, Hazard identification of inhaled nanomaterials: making use of short-term inhalation studies, /07/01 2012, *Arch. Toxicol.* 86 (7) (2012) 1137–1151, <https://doi.org/10.1007/s00204-012-0834-2>.
- W.-S. Cho, et al., Predictive value of in vitro assays depends on the mechanism of toxicity of metal oxide nanoparticles, /10/25 2013, *Part. Fibre Toxicol.* 10 (1) (2013) 55, <https://doi.org/10.1186/1743-8977-10-55>.
- W.-S. Cho, et al., Differential pro-inflammatory effects of metal oxide nanoparticles and their soluble ions in vitro and in vivo; zinc and copper nanoparticles, but not their ions, recruit eosinophils to the lungs, /02/01 2012, *Nanotoxicology* 6 (1) (2012) 22–35, <https://doi.org/10.3109/17435390.2011.552810>.

- [34] W.-S. Cho, et al., Progressive severe lung injury by zinc oxide nanoparticles; the role of Zn²⁺ dissolution inside lysosomes, /09/06 2011, Part. Fibre Toxicol. 8 (1) (2011) 27, <https://doi.org/10.1186/1743-8977-8-27>.
- [35] Y.-Y. Kao, Y.-C. Chen, T.-J. Cheng, Y.-M. Chiung, P.-S. Liu, Zinc oxide nanoparticles interfere with zinc ion homeostasis to cause cytotoxicity, Toxicol. Sci. 125 (2) (2011) 462–472, <https://doi.org/10.1093/toxsci/kfr319>.
- [36] N.R. Jacobsen, et al., Acute and subacute pulmonary toxicity and mortality in mice after intratracheal instillation of ZnO nanoparticles in three laboratories, /11/01/ 2015, Food Chem. Toxicol. 85 (2015) 84–95, <https://doi.org/10.1016/j.fct.2015.08.008>.
- [37] S. Sabella, et al., A general mechanism for intracellular toxicity of metal-containing nanoparticles, 10.1039/C4NR01234H, Nanoscale 6 (12) (2014) 7052–7061, <https://doi.org/10.1039/C4NR01234H>.
- [38] M.I. Greenberg, D. Vearrier, Metal fume fever and polymer fume fever, /04/21 2015, Clin. Toxicol. 53 (4) (2015) 195–203, <https://doi.org/10.3109/15563650.2015.1013548>.
- [39] R. Baumann, et al., Systemic serum amyloid A as a biomarker for exposure to zinc and/or copper-containing metal fumes, /01/01 2018, J. Expo. Sci. Environ. Epidemiol. 28 (1) (2018) 84–91, <https://doi.org/10.1038/jes.2016.86>.
- [40] K.E. Driscoll, P.J.A. Borm, Expert workshop on the hazards and risks of poorly soluble low toxicity particles (in eng), Inhal. Toxicol. 32 (2) (Feb 2020) 53–62, <https://doi.org/10.1080/08958378.2020.1735581>.
- [41] M.J. Bissell, Architecture is the message: the role of extracellular matrix and 3-D structure in tissue-specific gene expression and breast cancer (in eng), Pezcoller Found. J. 16 (29) (Oct 2007) 2–17.
- [42] C. Onursal, E. Dick, I. Angelidis, H.B. Schiller, C.A. Staab-Weijnitz, Collagen biosynthesis, processing, and maturation in lung ageing (in eng), Front. Med. 8 (2021) 593874, <https://doi.org/10.3389/fmed.2021.593874>.
- [43] T. Rozario, D.W. DeSimone, The extracellular matrix in development and morphogenesis: a dynamic view (in eng), Dev. Biol. 341 (1) (May 1 2010) 126–140, <https://doi.org/10.1016/j.ydbio.2009.10.026>.
- [44] J. Ma, B. Bishoff, R.R. Mercer, M. Barger, D. Schwegler-Berry, V. Castranova, Role of epithelial-mesenchymal transition (EMT) and fibroblast function in cerium oxide nanoparticles-induced lung fibrosis, /05/15/ 2017, Toxicol. Appl. Pharmacol. 323 (2017) 16–25, <https://doi.org/10.1016/j.taap.2017.03.015>.
- [45] N. Li, et al., Silica nanoparticle induces pulmonary fibroblast transdifferentiation via macrophage route: potential mechanism revealed by proteomic analysis, /10/ 01/ 2021, Toxicol. Vitro. 76 (2021) 105220, <https://doi.org/10.1016/j.tiv.2021.105220>.
- [46] C. Chang, Y. Pan, H. Du, X. Wang, X. Li, Serum amyloid A1 can be a novel biomarker for evaluating the presence and severity of acute coronary syndrome, /11/01/ 2020, Clin. Biochem. 85 (2020) 27–32, <https://doi.org/10.1016/j.clinbiochem.2020.08.005>.
- [47] M. Wiemann, A. Vennemann, U.G. Sauer, K. Wiench, L. Ma-Hock, R. Landsiedel, An *in vitro* alveolar macrophage assay for predicting the short-term inhalation toxicity of nanomaterials (in eng), J. Nanobiotechnol. 14 (Mar 5 2016) 16, <https://doi.org/10.1186/s12951-016-0164-2>.



Yunji Lee is a Ph.D. candidate in Materials Science and Engineering at Pohang University of Science and Technology (POSTECH), Republic of Korea. She earned her bachelor's degree in Chemical Engineering from Kyungpook National University in 2019. Leveraging her expertise in biomaterials, her research under the supervision of Dr. Sungjune Jung focuses on developing advanced *in vitro* lung models through bioprinting. Yunji's work holds promise for drug testing and disease research, particularly in the field of nanotoxicology.



Katie McAllister (MSci) earned her MSci in Pharmacology at the University of Strathclyde in 2024 having been awarded a BSc(Hons) in Pharmacology and Biochemistry from University of Strathclyde in 2023. Her master's thesis, conducted under the supervision of Dr Fiona Murphy, focused on evaluating *in vitro* models of the lungs for nanomaterial toxicity testing. Katie is currently working with Dr Murphy's group as a research scientist to optimize the incorporation of synthetic hydrogels in the development of animal-free *in vitro* models of the lung.



Dr. Hwa-Rim Lee is a research associate professor of Materials Science & Engineering in Pohang University of Science and Technology (POSTECH). Earlier he received Ph.D. degree in molecular neurophysiology from the School of Interdisciplinary Bioscience & Bioengineering (I-Bio, POSTECH) in 2016, focusing on regulatory mechanism in various physiological conditions of mammalian tissues. Since then, he has joined the Bioprinting and Printed Electronics laboratory (POSTECH) and is currently in charge of validation and application in *in vitro* human tissue models based on bioprinting technology as a research scientist.



Dr. Sungjune Jung is an associate professor at Department of Materials Science and Engineering in Pohang University of Science and Technology (POSTECH). He received his PhD degree in Manufacturing Engineering from University of Cambridge in 2007 and subsequently joined the Cavendish Laboratory of University of Cambridge. Before his PhD, he worked for Samsung Electronics, Digital Printing Division for 3 years. He has been leading the bio-printing and printed electronics laboratory since he joined POSTECH in 2013. His research focuses on 3D bioprinting and biofabrication as well as flexible printed electronics and biosensors.



Dr Fiona Murphy joined Strathclyde Institute of Pharmacy and Biomedical Sciences as a lecturer of Immunology and Pharmacology in September 2022. Fiona completed her PhD in particle toxicology at the University of Edinburgh with Prof Ken Donaldson, and postdoctoral research at the MRC Toxicology Unit in Leicester and Heriot-Watt University, Edinburgh using both *in vivo* and *in vitro* models to examine the inhalation hazard posed by particles and fibres including novel nanomaterials. Current research interests focus on the development of novel approaches for nanomaterial hazard assessment to reduce reliance on extensive *in vivo* case-by-case testing of new advanced materials.